buildings

MDPI

Article

Analysis of Out-of-Plane Displacements of a Light Steel Keel Fireproof Exterior Wall and Its Connection with the Steel Frame

Ang Wang [1,*], Ruiyuan Gao [1], Hao Li [2], Jing Li [1] and Ke Li [3]

[1] Civil Engineering and Construction Center, Huanghe Science and Technology University, Zhengzhou 450061, China; gry@hhstu.edu.cn (R.G.); ljhm202305052@hhstu.edu.cn (J.L.)
[2] Xi'an Noble Metal Material Co., Ltd., Xi'an 710018, China; lihao3547@gmail.com
[3] School of Civil Engineering, Zhengzhou University, Zhengzhou 450001, China; irwinlike@zzu.edu.cn
* Correspondence: wangang@hhstu.edu.cn

Abstract: Light steel keel fireproof exterior walls are one of the new composite walls that have been widely used in recent years. This paper analyzes the factors affecting the displacements of the connectors and wall panels and modifies the corresponding displacement model. ABAQUS was used to establish the simulation analysis of the L-shaped and special-shaped steel angle component, and the results were compared with the experimental model to verify the rationality. The effect of vertical keel spacing and layout, the number of special-shaped steel angles, the L-shaped steel angle thickness, and the number of self-tapping screws for L-shaped steel angles to steel beams were explored based on the validated finite element model. The calculation model was modified based on the results of the simulation. The results showed that the simulation results fit well with the experimental results, which verified the reliability of the finite element model. The number of connectors and the number of self-tapping screws are the main factors affecting the special-shaped and L-shaped steel angle components, respectively. By modifying the rotation constraint factor of the L-shaped steel angle and adding a discount factor for the wall panel, the accuracy of the associated displacement calculation model could be improved.

Keywords: light steel keel fireproof exterior wall; steel angle; displacement calculation model

check for updates

Citation: Wang, A.; Gao, R.; Li, H.; Li, J.; Li, K. Analysis of Out-of-Plane Displacements of a Light Steel Keel Fireproof Exterior Wall and Its Connection with the Steel Frame. *Buildings* **2024**, *14*, 1564. https://doi.org/10.3390/buildings14061564

Academic Editor: Binsheng (Ben) Zhang

Received: 2 April 2024
Revised: 19 May 2024
Accepted: 24 May 2024
Published: 28 May 2024

Copyright: © 2024 by the authors. Licensee MDPI, Basel, Switzerland. This article is an open access article distributed under the terms and conditions of the Creative Commons Attribution (CC BY) license (https://creativecommons.org/licenses/by/4.0/).

1. Introduction

Assembled steel structure systems have good economic and environmental benefits, and their main advantages include a high degree of assembly, a light weight, and good seismic performance [1–4]. The assembled steel structure's exterior maintenance walls can be categorized into masonry infill walls, single material walls, and composite walls according to the material. Among these, the composite wall is assembled by two or more materials; it is more environmentally friendly, has a higher degree of assembly, and the construction process is quite simple [5,6]. The light weight and high strength of the light steel keel makes it a better match for fireproofing materials, and light steel keel composite walls have recently been widely used. Common fireproofing materials include gypsum, calcium silicate, and phenolic fibers, and all of these materials have fire-resistant and heat-insulating properties. In fire scenarios, the light steel keel can still be in a relatively normal working environment and keep its load-bearing capacity [7,8].

To ensure that different materials can work well with the main body of the steel structure, a large number of studies have been carried out on the performance of the connection between the steel frame and the enclosing wall [9–14]. Stability is the first factor to be considered when connecting the wall to the steel structure. In addition, the connectors should be easy to install and should not be too costly. Geng et al. proposed an external connection scheme to enhance the assembly of the light steel keel wall and verified its reliability under normal use conditions versus seismic conditions [15]. Tang et al. proposed a new filled-bolt connection, which exhibited satisfactory mechanical properties [16]. Steel

angles have been proven to play an important role in connecting steel frames to enclosing walls [17]. This study focused on two types of connections, L-shaped and special-shaped steel angles, and explored the effects of the spacing and layout of vertical keels, the number of special-shaped steel angle connectors, the thickness of L-shaped steel angles, and the number of self-tapping screws used to connect the enclosing wall to the steel beams. This study could provide a useful reference for the selection and layout of the light steel keel walls and connections.

Displacement under external loading conditions is a visual reflection of the performance of the walls. Wind load is one of the most important factors affecting the out-of-plane displacement of walls, especially for high buildings. Under the influence of strong winds, there is a risk of partial or complete overturning of the walls, which would seriously threaten the safety of life and property [18]. On the other hand, in earthquake-prone regions, the impact of seismic forces on walls cannot be ignored. Without a reasonable seismic design, a large number of buildings would crack and collapse during earthquakes [19]. To reduce the risk of wall instability, a lot of structural displacement monitoring methods have been developed. Current methods are mainly divided into two categories: one is the displacement monitoring technology based on sensors, and the other is based on vision, and both can provide insight into the displacement of a wall over a period of time [20]. Obviously, it is much more valuable to study the prediction of the displacement of the wall before construction is carried out. Experiments and numerical simulations are currently the main methods used to predict the displacement of light steel keel walls and connections [21–26]. Telue et al. investigated the force properties of walls under axial loads by conducting a large number of experiments [27]. Tian et al. explored the effects of wall panel type, screw spacing, and load type on wall performance based on experiments [28]. Wu et al. developed a refined model of light steel keel composite walls and verified the accuracy of the model through experiments [25]. Compared to experimental methods, numerical simulation is a much more efficient method. Finite element analysis (FEA) is currently the most widely used numerical simulation approach, but for some complex structures, finite element simulation is still a time-consuming process, and the accuracy is difficult to guarantee. Overall, experimental and simulation analyses usually consume a lot of economic and time costs, so it is necessary to propose an accurate and reliable theoretical calculation model. In this paper, based on previous studies, more accurate displacement calculation models for walls and connectors are proposed.

To summarize, this paper focused on two connection forms of special-shaped and L-shaped steel angles. Various displacement influence factors were analyzed, and more accurate displacement calculation models were proposed. The research in this paper can provide an important reference for the layout of light steel keel walls and connectors. More accurate theoretical calculation models can provide a more efficient option for the displacement analysis of walls and connections.

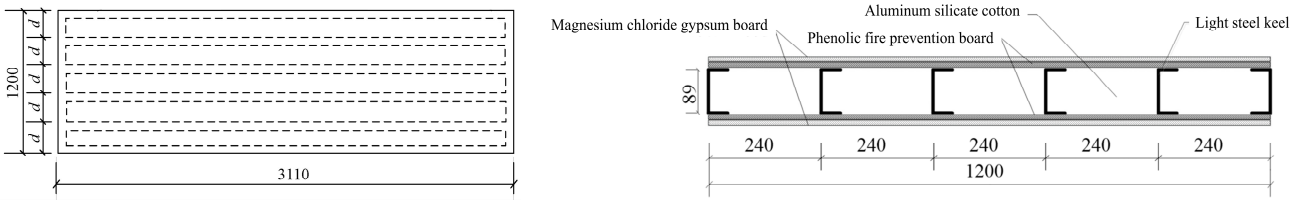
2. Materials and Methods

2.1. Finite Element Modeling and Validation

(1) Modelling of geometry

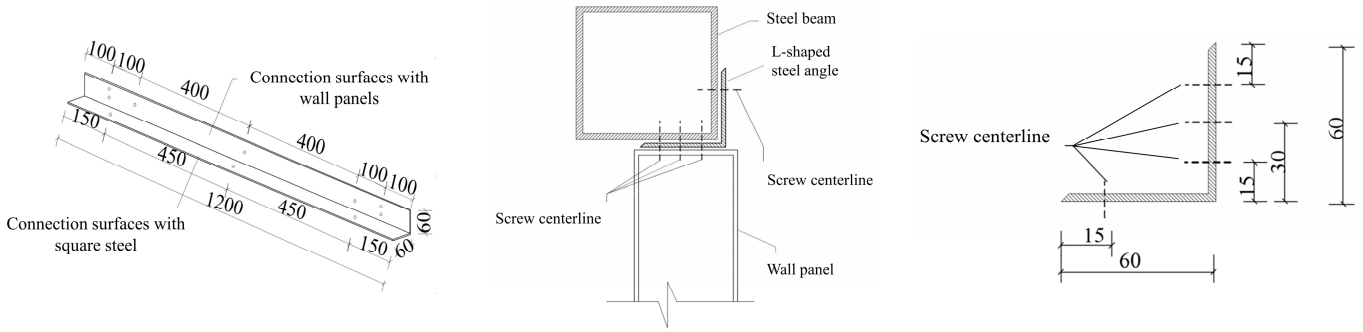
The FEA process was based on the ABAQUS 2023 software. Firstly, the geometry was modeled based on common light steel keel exterior wall characteristics. The dimensions and material composition of the wall are shown in Figure 1. The width of the wall panel is 1200 mm, and the length is 3110 mm. The size of the C-type light steel keel in the wall panel is h × b × c × t = 89 mm × 41 mm × 8 mm × 0.8 mm, where h, b, c and t are the cross-section height of the steel keel, the width of the flange, the width of the rolled edge, and the thickness, respectively, and the spacing of the C-type steel keel, d, is 240 mm. The dimensions of the phenolic fire prevention board and magnesium chloride gypsum board are both l × b × t = 3110 mm × 1200 mm × 4 mm, where l, b and t are the length, width and thickness, respectively. To study the out-of-plane displacements of the wall under different connections, two connection methods were designed: one

through-length L-shaped steel angle connection for QB_1 (Figure 2) and one special-shaped steel angle connection for QB_2 (Figure 3). Steel angles, wall panels and steel beams were connected to each other with self-tapping screws. The steel beam cross-section dimensions are 150 mm × 150 mm × 8 mm × 8 mm. Finally, a geometric model was built, as shown in Figure 4.



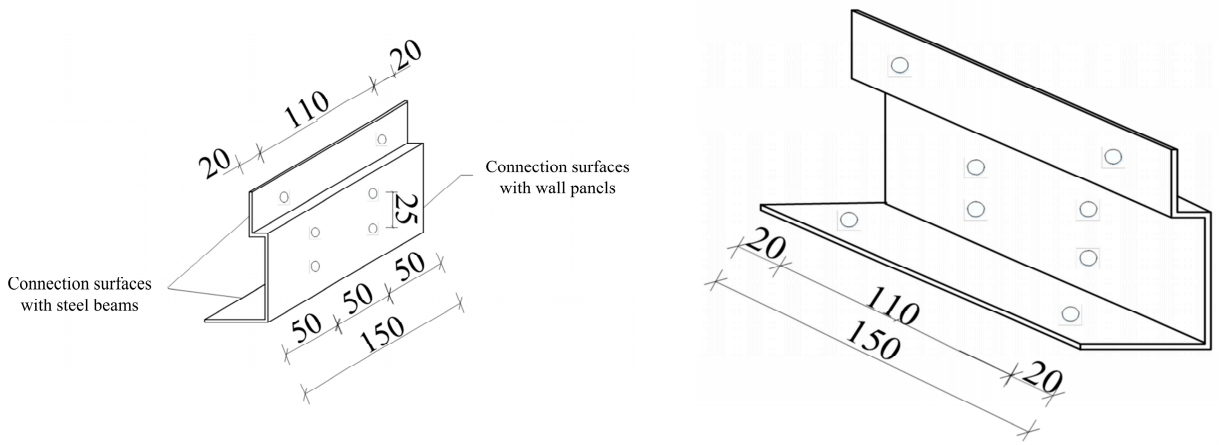
(**a**) (**b**)

Figure 1. The dimensions and material composition of the wall: (**a**) plan schematic; (**b**) section schematic.



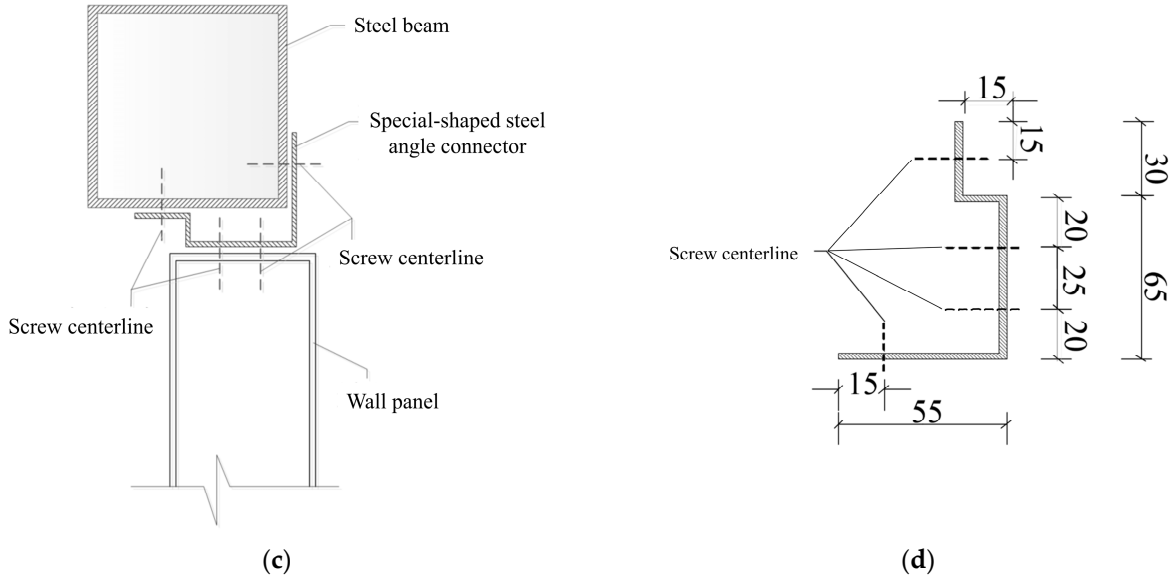
(**a**) (**b**) (**c**)

Figure 2. Schematic diagrams: (**a**) L-shaped steel angle and screw holes; (**b**) L-shaped steel angle connection; and (**c**) L-shaped steel angle cross-section and screw hole locations (units: mm).



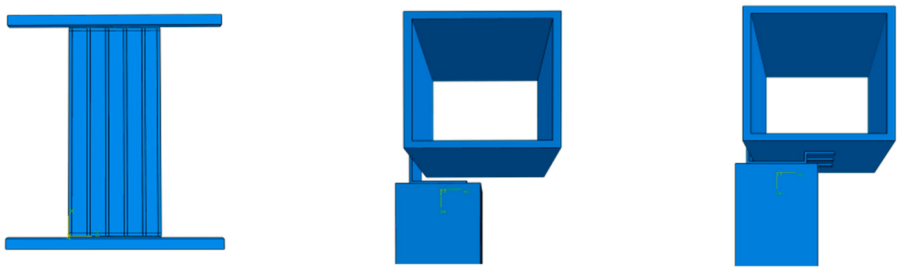
(**a**) (**b**)

Figure 3. *Cont.*



(**c**) (**d**)

Figure 3. The schematic diagrams: (**a**) outer face of the special-shaped steel angle; (**b**) inside face of the special-shaped steel angle; (**c**) special-shaped steel angle connection; (**d**) special-shaped steel angle cross-section and screw hole locations (units: mm).



(**a**) (**b**) (**c**)

Figure 4. Finite element geometric model: (**a**) overall model; (**b**) QB1 connection model; (**c**) QB2 connection model.

(2) Material properties

The keel of light steel keel fireproof exterior wall is made of cold-formed thin-walled steel, covered with phenolic fire prevention board and magnesium chloride gypsum board, and filled with aluminum silicate cotton inside. The materials of steel beams and steel angle connectors are Q235 ordinary carbon steel and Q345 ordinary carbon steel, respectively. The cold-formed thin-walled steel, Q235 ordinary carbon steel, and Q345 ordinary carbon steel are regarded as elastic–plastic materials. The phenolic fire-prevention board and magnesium chloride gypsum board were considered as elastic material. The parameters of the elastic and plastic stages of the elastic–plastic material during the simulation are shown in Tables 1 and 2, respectively. It should be noted that isotropic hardening of the materials in the plastic stage was also considered. For elastic materials, when the external load exceeds their strength, the material will fracture and stop working. The relevant parameters are presented in Table 3.

(3) Unit type and mesh size selection

For the light steel keel, phenolic fire prevention board, and magnesium chloride gypsum board, the S4R unit was applied. The S4R unit can be used for modeling thin or thick shell structures with reduced integration. It includes hourglass mode control and allows for finite film strains. For the L-shaped and special-shaped steel angle and the steel

beams, the unit type is C3D8R. The C3D8R unit is less prone to shear self-locking under bending loads and has advantages in solving displacement problems. In addition, by using C3D8R units, the accuracy of the analysis would rarely be affected when there is a twisting deformation of the meshes.

Table 1. Elastic–plastic material parameters at the elastic stage.

Materials	Modulus of Elasticity (MPa)	Yield Strength (MPa)	Poisson's Ratio
Cold-formed thin-walled steel	171,000	293.7	0.31
Q235 ordinary carbon steel	210,000	235	0.30
Q345 ordinary carbon steel	210,000	345	0.3

Table 2. Elastic–plastic material parameters at the plastic stage.

Materials	True Stress (MPa)	True Plastic Strain
Cold-formed thin-walled steel	294.19	0
	300.76	0.0146230
	338.43	0.0542114
	371.56	0.0836651
	436.39	0.1885053
Q235 ordinary carbon steel	235.2628	0
	431.876	0.075555
Q345 ordinary carbon steel	345.5663	0
	537.7247	0.071099

Table 3. Elastic material parameters.

Materials	Modulus of Elasticity (MPa)	Strength (MPa)	Poisson's Ratio
Phenolic fire-prevention board	34,500	391.2	0.29
Magnesium chloride gypsum board	1500	1.13	0.38

The determination of mesh size Is an Important step In FEA. In general, the smaller the mesh size, the more accurate the simulation results. However, smaller mesh sizes also consume longer computation time, so reaching a balance between accuracy and computational cost is a difficult subject. With reference to previous studies [29], the choice of mesh size could be related to the surface area of the component, and the following equations are given:

$$\text{Coarse mesh size} = 0.049\ (\text{Overall surface area of the component})^{1/2} \quad (1)$$

$$\text{Fine mesh size} = 0.0245\ (\text{Overall surface area of the component})^{1/2} \quad (2)$$

Finally, based on the results of the formulas, the mesh size of the light steel keel and the connectors was taken as 10 mm. For the phenolic fire protection board and steel frame, the mesh size was taken as 50 mm.

(4) Interactions and constraints

Tie binding constraints were defined between the horizontal and vertical keels to form the keel frame. In addition, Tie binding constraints were also defined between the keel frame, phenolic fire prevention board, and magnesium chloride gypsum board. After determining the position of the self-tapping screws, the tie-binding constraints were defined again. The peripheral units at the self-tapping screws were coupled by shifts while setting up contact between the steel angle and the steel demand and wall panels in the form of normal hard contact with tangential friction. In addition, fixed constraints were applied

at 4 corners on the steel beams, and the model as a whole could be vertically displaced (Figure 5).

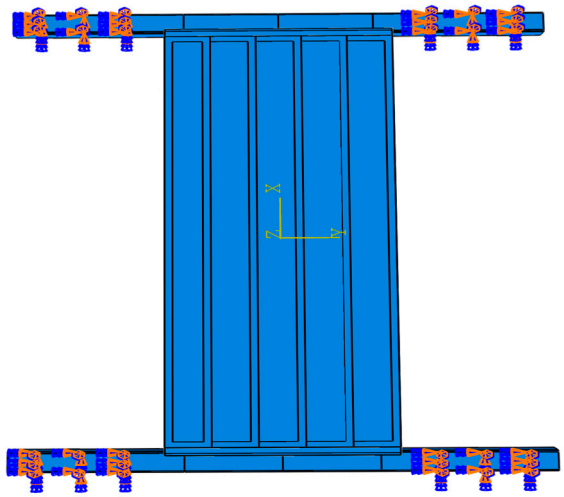


Figure 5. Schematic diagram of the constraint.

(5) Loading procedure

In this paper, to simulate wind loads, a graded loading procedure was set up with a load of 0.402 kN/m^2 per level. A total of eight levels of loadings (maximum of 3.216 kN/m^2) were used for the L-shaped steel angle component. Ten levels of loadings (maximum of 4.020 kN/m^2) were used for the special-shaped steel angle component.

(6) Validation

Taking into account the above geometrical models, material properties, connection methods, etc., the corresponding experimental models were developed to verify the validity of the FEA models (Figure 6). The loading procedure was realized by static stacking 10 kg gravel bags. Fifteen bags per level were required, evenly spread, keeping 20 mm spacing between bags and bags, to prevent the sandbags from the force of accumulation of arching. Three displacement gauges were arranged at the mid-span of the wall panel and at the L-shaped steel angle connection (or special-shaped angle connection) separately to measure the settlement of the wall panel and the connectors.



(**a**) (**b**)

Figure 6. Schematic diagrams: (**a**) experimental setup; (**b**) loading process.

2.2. Simulation Scheme

To analyze the effects of different factors on the displacements of wall panels and connections under loading conditions, the simulation scheme shown in Table 4 was pro-

posed. The special-shaped angle connection components mainly considered the number of connectors, the keel layout, and the keel spacing. The L-shaped angle connection components mainly considered the steel angle thickness, the keel layout, the keel spacing, and the number of self-tapping screws used in connection with steel beams. The symmetrical layout is symmetrical in the direction of the keel opening, as shown in Figure 7.

Table 4. The simulation scheme.

Number	Connector Thickness (mm)	Steel Angle Type	Keel Layout	Keel Spacing (mm)	Number of Self-Tapping Screws for Connectors to Steel Beams	Number of Self-Tapping Screws for Connectors to Wall Panels
LA-1	2.5	L-shaped	Normal	300	3 unilateral	8 unilateral
LA-2	2.5	L-shaped	Normal	240	3 unilateral	8 unilateral
LA-3	2.5	L-shaped	Normal	200	3 unilateral	8 unilateral
LB-1	1.5	L-shaped	Asymmetrical	240	3 unilateral	8 unilateral
LB-2	2	L-shaped	Asymmetrical	240	3 unilateral	8 unilateral
LB-3	2.5	L-shaped	Asymmetrical	240	3 unilateral	8 unilateral
LC-1	2.5	L-shaped	Asymmetrical	240	3 unilateral	8 unilateral
LC-2	2.5	L-shaped	Asymmetrical	240	4 unilateral	8 unilateral
LC-3	2.5	L-shaped	Asymmetrical	240	5 unilateral	8 unilateral
YA-1	2.5	Special-shaped (3 unilateral)	Normal	300	12 unilateral	12 unilateral
YA-2	2.5	Special-shaped (3 unilateral)	Normal	240	12 unilateral	12 unilateral
YA-3	2.5	Special-shaped (3 unilateral)	Normal	200	12 unilateral	12 unilateral
YB-1	2.5	Special-shaped (2 unilateral)	Asymmetrical	240	8 unilateral	8 unilateral
YB-2	2.5	Special-shaped (3 unilateral)	Asymmetrical	240	12 unilateral	12 unilateral
YB-3	2.5	Special-shaped (4 unilateral)	Asymmetrical	240	16 unilateral	16 unilateral

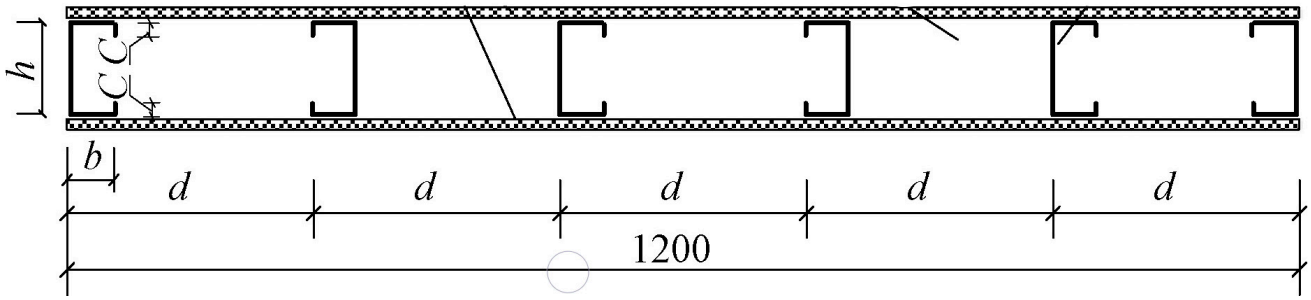


Figure 7. The diagram of the symmetrical keel layout.

2.3. Displacement Calculation Model

Due to the complex structure of steel angle connectors and light steel keel walls, there is no recognized accurate displacement calculation model [30]. Based on the structural mechanics and previous research, the following preliminary calculation model for the displacements of special-shaped steel angle connectors, L-shaped steel angle connectors, and wall panels at mid-span was given below [31–33]. Subsequently, more accurate models would be revised based on multiple sets of numerical simulations.

(1) Displacement calculation model for L-shaped steel angle connectors

The calculation sketch of the L-shaped steel angle is shown in Figure 8, and the displacements of the connectors under out-of-plane loading can be calculated according to the following formulas:

$$\Delta a = \frac{w_k b l_0}{2 k_a D_0} \tag{3}$$

$$k_a = 0.45 \frac{n_t}{t_a} - 0.359 \leq 1 \tag{4}$$

$$D_0 = \frac{3EI}{c^3} \tag{5}$$

where w_k is the load value; b is the wall plate section width; l_0 is the calculated span of the wall panel; k_a is the rotation constraint coefficient of the L-shaped steel angle connectors; n_t is the number of screws connecting L-shaped steel angle connectors to steel beams; t_a is the thickness of the L-shaped steel angle connectors; D_0 is the lateral displacement stiffness of c with the stiffness as the value of the external force required to cause a unit deformation of an object; E is the modulus of elasticity of the connectors; I is the moment of inertia of the connectors; and c is the distance from the center of the steel beam connecting screws to the line of shear effect.

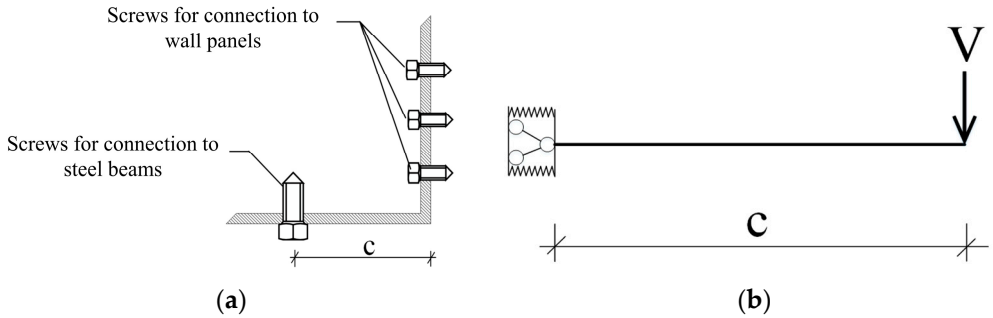


Figure 8. Schematic diagrams: (**a**) L-shaped steel angle connection; (**b**) calculation of forces.

(2) Displacement calculation model for the special-shaped steel angle connectors

The calculation sketch of the special-shaped steel angle is shown in Figure 9, and the displacements of connectors under out-of-plane loading can be calculated according to the following formulas:

$$\Delta_b = \frac{w_k b l_0}{2 K_b D_0} \tag{6}$$

$$K_b = 1.61 \sum_{i=1}^{N} k_{bi} - 0.14 \tag{7}$$

$$k_b = 0.06 \frac{n_1 n_2}{t_b} \leq 1 \tag{8}$$

where w_k is the load value; b is the wall panel section width; l_0 is the calculated span of the wall panel; K_b is the overall rotation constraint coefficient of the special-shaped steel angle connectors; D_0 is lateral displacement stiffness of AB; N is the number of the connectors; k_b is the rotation constraint coefficient of a single special-shaped steel angle connector; n_1 is the number of extraction-resistant screws; n_2 is the number of shear-resistant screws; and t_b is the thickness of the special-shaped steel angle connectors.

(3) Displacement calculation model for the wall panel

The displacement of the wall panel under out-of-plane loading can be calculated according to the following formulas:

$$\Delta = \frac{5 w_k b l_0^4}{384 B_S} \tag{9}$$

$$B_S = E_S\left(I_S + mI_1'\right) \tag{10}$$

where w_k is the load value; b is the wall plate section width; l_0 is the calculated span of the wall panel; B_s is the combined stiffness of the wall panel; E_s is the modulus of elasticity of the light steel keel; I_s the sum of the moments of inertia of the keel; m is the mask combination effect coefficient; and I'_1 is the moment of the inertia of the phenolic panels.

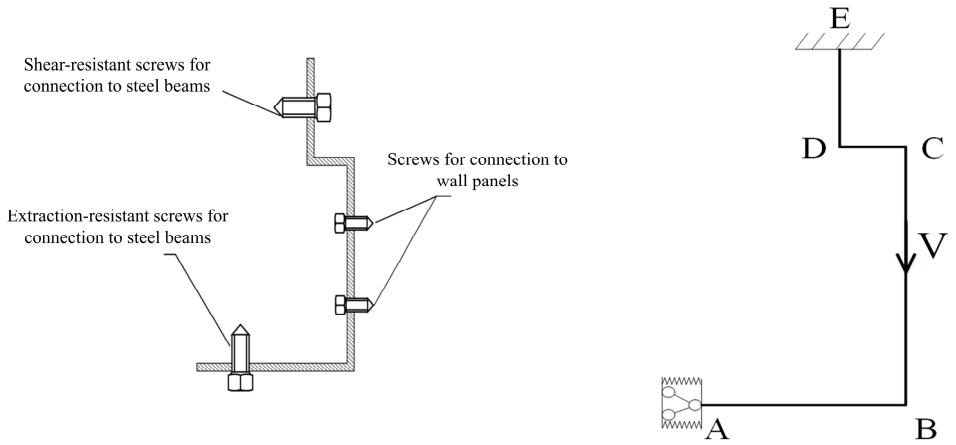


Figure 9. Schematic diagrams: (**a**) special-shaped steel angle connection; (**b**) calculation of forces.

3. Results

3.1. Comparison of Simulation and Experimental Results

Table 5 shows the experimental results and simulation results of the two experimental components under certain loading conditions. The load–displacement curves of the wall panels and the connectors are shown in Figure 10. As can be seen from the figure, the curves obtained from FEA and experiments are basically consistent. According to the FEA results, the displacements of the components increased linearly with the load, indicating that the components were all in an elastic state. In contrast, although the experimental results have similar trends, the loading–displacement process is significantly more complex. The simulation inaccuracy of the curves of QB_1 is smaller than that of QB_2, and the inaccuracies between the experimental results and the FEA results are all within 20%. The FEA values are smaller than the experimental values, which might be due to the fact that FEA ignored the slip between the phenolic panels and the light steel keel, which increased the stiffness of the wall panels.

Table 5. Experimental and FEA values of the displacements for the components.

Components	FEA Values (F)	Experimental Values (E)	F/E
Connectors for QB_1	3.16	2.97	1.06
Connectors for QB_2	0.57	0.63	0.90
Wall panel for QB_1	9.42	10.25	0.92
Wall panel for QB_2	9.56	11.7	0.82

3.2. Analysis of Displacement Influencing Factors

3.2.1. L-Shaped Steel Angle Connectors and Wall Panels

(1) Keel spacing

The load–displacement curves for the LA group are shown in Figure 11. The wall panel displacement under the same load decreased with the decreasing keel spacing, indicating that decreasing the keel spacing could improve the out-of-plane stiffness of the wall panel to

some extent, but the effect is not obvious. The load–displacement curves of the connectors basically coincide, indicating that reducing the keel spacing has no effect on the stiffness of the connectors.

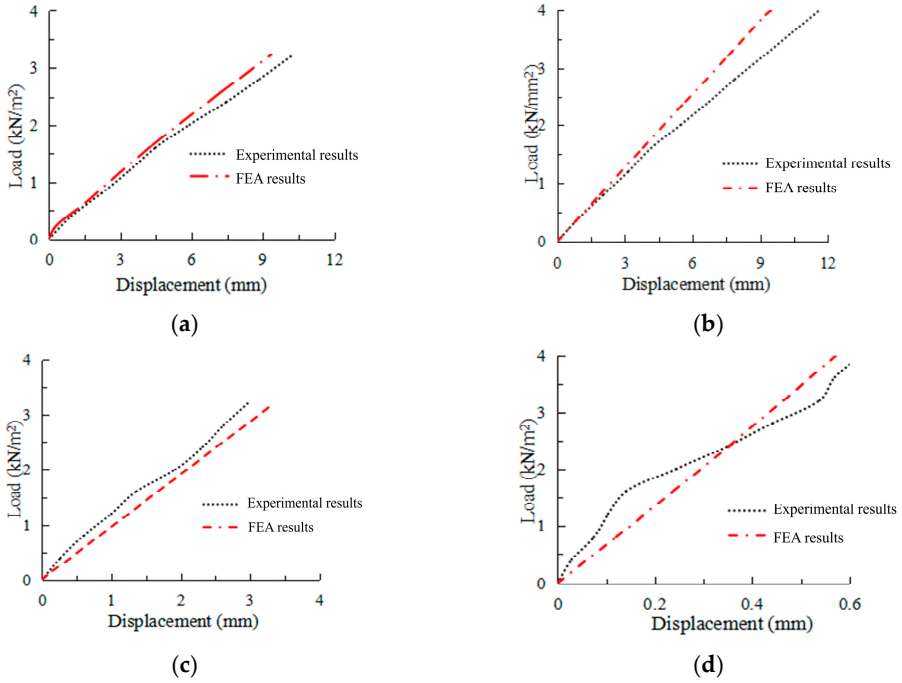


Figure 10. Load–displacement curves: (**a**) the connectors for QB_1; (**b**) the connectors for QB_2; (**c**) the wall panel for QB_1; and (**d**) the wall panel for QB_2.

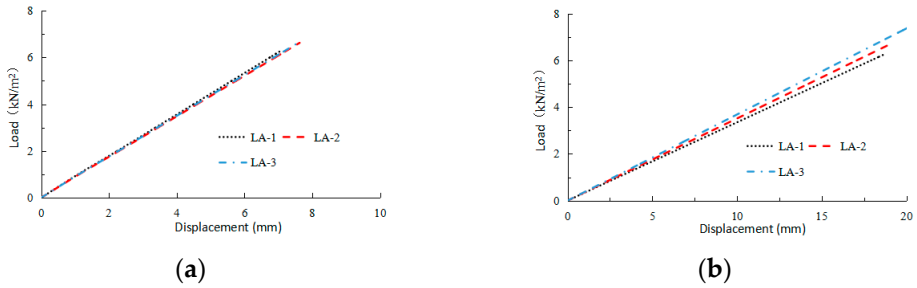


Figure 11. Load–displacement curves for the LA group: (**a**) the L-shaped steel angle connectors; and (**b**) the wall panel.

(2) Thickness of the L-shaped steel angles

The load–displacement curves for the LB group are shown in Figure 12. The displacements of the wall panel and the L-shaped steel angle connectors under the same load decreased with the increasing thickness of the connectors, indicating that the thicker the thickness of the connection, the higher the stiffnesses of the wall panel and the connectors. When the thickness of the connectors increased from 1.5 mm to 2 mm, the effect on the stiffness of the wall panels and connectors was greater than when the thickness increased from 2 mm to 2.5 mm.

(3) Number of screws connecting the connector to the steel beams

The load–displacement curves for the LC group are shown in Figure 13. The displacement of the wall panel and the L-shaped steel angle connectors under the same load decreased with the increasing number of screws connecting the connector to the steel beams, indicating that the more screws used, the higher the stiffness of the wall panel and the connectors. When the number of screws increased from 3 to 4, the effect on the stiffness

of the wall panels and connectors was greater than when the number of screws increased from 4 to 5.

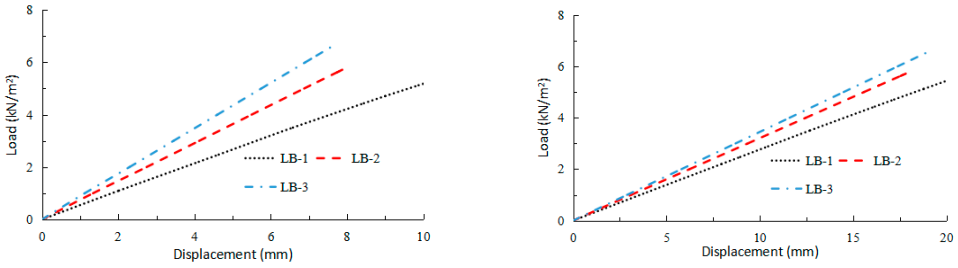


Figure 12. Load–displacement curves for the LB group: (**a**) the L-shaped steel angle connectors; and (**b**) the wall panel.

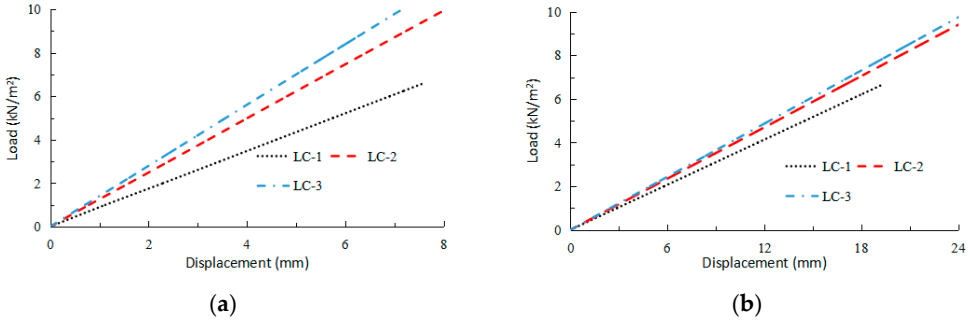


Figure 13. Load–displacement curves for the LC group: (**a**) the L-shaped steel angle connectors; (**b**) the wall panel.

(4) Layout of the keel

Comparing LA-2 and LB-3, the load–displacement curves of the wall panels and connectors basically coincided, so changing the keel layout has no significant effect on the stiffness of the wall panels and connectors.

3.2.2. Special-Shaped Connectors and Wall Panels

(1) Keel spacing

The load–displacement curves for the YA group are shown in Figure 14. The wall panel displacement under the same load decreased with the decreasing keel spacing, indicating that decreasing the keel spacing could improve the out-of-plane stiffness of the wall panel to some extent, but the effect is not obvious. The load–displacement curves of the connectors basically coincide, indicating that reducing the keel spacing has no effect on the stiffness of the connectors.

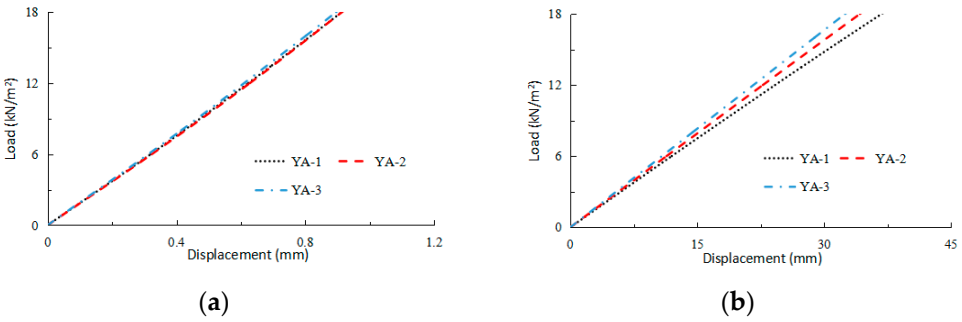
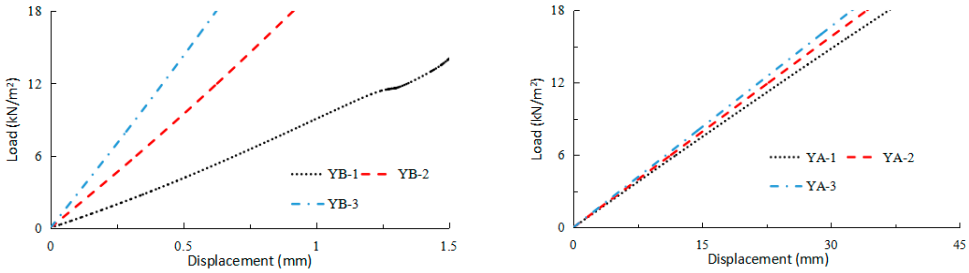


Figure 14. Load–displacement curves for the YA group: (**a**) the special-shaped steel angle connectors; and (**b**) the wall panel.

(2) Number of special-shaped steel angle connectors

The load–displacement curves for the YB group are shown in Figure 15. The displacements of the wall panel and the special-shaped steel angle connectors under the same load decreased with the increasing number of the special-shaped steel angle connectors, indicating that the more connectors used, the higher the stiffness of the wall panel and the connectors. When the number of connectors increased from two to tree, the effect on the stiffness of the wall panels and connectors was greater than when the number of connectors increased from three to four.



(**a**) (**b**)

Figure 15. Load–displacement curves for the YB group: (**a**) the special-shaped steel angle connectors; and (**b**) the wall panel.

(3) Layout of the keel

Comparing YA-2 and YB-3, the load–displacement curves of the wall panels and connectors basically coincided, so changing the keel layout has no significant effect on the stiffness of the wall panels and connectors.

3.3. Displacement Model Modification

3.3.1. Displacement Model Modification for Connectors

The rotation constraint coefficients and displacements obtained from the pre-prepared displacement calculation model are listed in Table 6 along with the simulated values. The results show that the theoretically calculated values were in good agreement with the simulation values, except for LC-2 and LC-3. The theoretical calculations for LC-2 and LC-3 are on the small side, which may be due to the fact that Equation (5) overestimated the contribution of the number of screws to the stiffness of the connectors.

Table 6. The calculated and simulated values of the connector displacements.

Number	K_b (k_α)	Extreme Load (kN/m^2)	Simulated Displacement (S) (mm)	Theoretically Calculated Displacement (T) (mm)	S/T
LA-1	0.181	5.5	5.51	5.35	1.029
LA-2	0.181	5.7	5.71	5.55	1.029
LA-3	0.181	6.5	6.12	6.33	0.967
LB-1	0.541	5.4	8.91	8.14	1.095
LB-2	0.316	5.5	6.61	5.99	1.104
LB-3	0.181	5.8	5.81	5.64	1.029
LC-1	0.181	5.8	5.81	5.64	1.029
LC-2	0.361	7.5	5.70	3.67	1.555
LC-3	0.541	9.2	5.75	2.98	1.928
YA-1	0.348	9.7	0.58	0.65	0.899
YA-2	0.348	12.1	0.73	0.80	0.909
YA-3	0.348	10.4	0.60	0.69	0.871
YB-1	0.185	5.1	0.74	0.89	0.832
YB-2	0.348	12.5	0.76	0.83	0.917
YB-3	0.510	14.7	0.66	0.67	0.998

Substituting the simulation values of the displacement of the connectors of the LC group into Equation (5), the rotation constraint coefficient k_α values of LC-1, LC-2, and LC-3 were inverted to 0.181, 0.232, and 0.281, respectively. Combining the rotation constraint coefficients obtained from theoretical calculations of the LA and LB groups of the connectors, k_α was modified as follows:

$$k_a = \frac{0.125n_t + 0.976}{t_a} - 0.359 \leq 1 \tag{11}$$

The k_a values and the corresponding displacements were recalculated based on the modified equations and compared with the simulated values. The results are shown in Table 7. The results showed that the recalculated values are all within the 10% inaccuracy, indicating the accuracy of the modified displacement model.

Table 7. The recalculated and simulated values of the connector displacements.

Number	k_α	Simulated Displacement (S) (mm)	Theoretically Calculated Displacement (T) (mm)	S/T
LA-1	0.181	5.353	5.51	1.029
LA-2	0.181	5.548	5.71	1.029
LA-3	0.181	6.326	6.12	0.967
LB-1	0.542	8.122	8.91	1.097
LB-2	0.317	5.968	6.61	1.108
LB-3	0.181	5.643	5.81	1.029
LC-1	0.181	5.643	5.81	1.029
LC-2	0.231	5.732	5.7	0.994
LC-3	0.281	5.743	5.75	1.001

3.3.2. Displacement Model Modification for Wall Panels

The combined stiffness of the wall panel and displacement obtained from the pre-prepared displacement calculation model are listed in Table 8 along with the simulated values. As shown in the table, the theoretically calculated values of wall panel displacements are generally larger than the simulated values, which may be due to the assumption of ideal articulated constraints between the wall panels and the connectors in the calculations, whereas the screws between the wall panels and the connectors in the numerical analyses could provide the rotational constraints at the panel ends and the setup of contacts between the transverse keel at the end of the wall panel and the connectors limited the rotational displacements at the end of the panels so that the theoretical results of the calculations are on the large side.

A discount factor γ is introduced to discount the values calculated by the theoretical formula:

$$\Delta = \gamma \frac{5w_k b l_0^4}{384 B_S} \tag{12}$$

Substituting the simulation values of the wall panel displacement to fit γ, the final γ was determined to be 0.71.

$$\Delta = 0.71 \times \frac{5w_k b l_0^4}{384 B_S} \tag{13}$$

The displacements were recalculated based on the modified equations and compared with the simulated values. The results were shown in Table 9. The results showed that the recalculated values are all within 10% inaccuracy, indicating the accuracy of the modified displacement model.

Table 8. The calculated and simulated values of the wall panel displacements.

Number	Combined Stiffness ($kN \cdot m^2$)	Extreme Load (kN/m^2)	Simulated Displacement (S) (mm)	Theoretically Calculated Displacement (T) (mm)	S/T
LA-1	617.21	5.50	10.24	13.03	0.786
LA-2	568.08	5.70	9.96	14.67	0.679
LA-3	617.21	6.50	10.85	15.39	0.705
LB-1	568.08	5.40	9.36	13.89	0.674
LB-2	568.08	5.50	9.57	14.15	0.676
LB-3	568.08	5.80	10.13	14.92	0.679
LC-1	568.08	5.80	10.13	14.92	0.679
LC-2	568.08	7.52	13.10	19.34	0.677
LC-3	568.08	9.16	15.98	23.57	0.678
YA-1	514.66	9.73	18.94	27.63	0.685
YA-2	568.08	12.10	22.21	31.13	0.713
YA-3	617.21	10.40	18.37	24.63	0.746
YB-1	568.08	5.11	10.80	13.15	0.821
YB-2	568.08	12.50	22.91	32.16	0.712
YB-3	568.08	14.70	26.69	37.82	0.706

Table 9. The recalculated and simulated values of the wall panel displacements.

Number	Combined Stiffness ($kN \cdot m^2$)	Extreme Load (kN/m^2)	Simulated Displacement (S) (mm)	Theoretically Calculated Displacement (T) (mm)	S/T
LA-1	617.21	5.50	10.24	11.09	0.923
LA-2	568.08	5.70	9.96	10.41	0.957
LA-3	617.21	6.50	10.85	10.93	0.993
LB-1	568.08	5.40	9.36	9.87	0.948
LB-2	568.08	5.50	9.57	10.05	0.952
LB-3	568.08	5.80	10.13	10.60	0.956
LC-1	568.08	5.80	10.13	10.60	0.956
LC-2	568.08	7.52	13.10	13.73	0.954
LC-3	568.08	9.16	15.98	16.73	0.955
YA-1	514.66	9.73	18.94	19.62	0.965
YA-2	568.08	12.10	22.21	22.11	1.005
YA-3	617.21	10.40	18.37	17.49	1.050
YB-1	568.08	5.109	10.80	9.33	1.158
YB-2	568.08	12.50	22.91	22.84	1.003
YB-3	568.08	14.70	26.69	26.86	0.994

4. Discussion

4.1. Analysis of Factors Affecting the Displacements of Connectors and Wall Panels

Light steel keel fireproof exterior walls are one of the main types of current assembled structural walls. The connection performance of the wall and the steel frame directly determines the effect of the wall and the main structure of the building working together. Heimbs et al. compared the effects of different forms of L-shaped steel angle nodes and bolted nodes and analyzed the corresponding damage modes [17]. Zhang et al. designed a novel connection using a U-shaped connector to connect the wall to the steel frame, which was shown to have good performance [34]. The performance of the connection between the wall and the steel frame is determined by multiple factors [35]. A systematic analysis of the multiple influence factors on the performance of wall and steel beam connections can provide an important reference for the selection and placement of connectors and wall panels. This paper focused on two types of connections, including L-shaped steel angles and special-shaped steel angles. For the L-shaped steel angles, the spacing and arrangement of the keels, the thickness of the L-shaped steel angles, and the number of screws connecting the L-shaped steel angles to the steel beams were considered. For the

special-shaped steel angles, the spacing and arrangement of the keels and the number of connectors were taken into account. The displacements of the connection and wall panels under loading conditions were regarded as the evaluation index of the performance of the connections. The results showed that the number of screws connecting the L-shaped steel angles to the steel beams and the number of special-shaped steel angle connectors are decisive factors in improving the performance of the connection between the wall and the steel frame. However, when the number of screws and connectors reached some thresholds, the performance enhancement will no longer be evident.

4.2. Modification of the Displacement Model for Connectors and Wall Panels

The keel in the light steel keel fireproof exterior wall is generally rolled from 0.5–1.5 mm galvanized coils, and the thin thickness and complex structure make the theoretical calculation difficult. At present, most studies on the connection between light steel keel fireproof exterior walls and steel frames are based on experiments and finite element simulation analysis [36]. However, compared to experiments and finite element simulations, theoretical calculation is a method that can be applied and generalized more easily. In this paper, on the basis of the previous research and the theory of structural mechanics, the corresponding displacement calculation models were pre-proposed for L-shaped steel angle connectors, special-shaped steel angle connectors and wall panels. The computational results of these models were then compared with the simulation results, and further modifications were made. The results showed that the pre-proposed displacement model for L-shaped steel angle connectors overestimated the contribution of screws to the rotational stiffness; the rotation constraint coefficient was therefore modified. The ideal articulation constraints assumed by the pre-proposed wall panel displacement model would bias the calculations, and a discount factor was added accordingly. The computational results of the modified model were all in good agreement with the simulation results, indicating that the modified model can provide a fast and accurate new approach for obtaining the displacements of connectors and wall panels.

4.3. Limitations

The present study focused on two connection forms of special-shaped and L-shaped steel angles, different displacement effect factors were investigated and more accurate displacement calculation models were introduced. For further promotion of the light steel keel exterior walls, there are still some limitations that need to be addressed. Compared to traditional walls, light steel keel exterior walls usually have a higher cost and are highly dependent on industrial support. In addition, the lightweight characteristics of light steel keel exterior walls make it difficult to ensure their structural integrity in seismic and strong-wind environments. In future studies, the optimization of the structural design and the use of high-strength materials can make it easier to extend the use of light steel keel exterior walls to earthquake-prone and windy areas. On the other hand, the selection of wall materials should also take durability and environmental friendliness into consideration to further enhance their life cycle.

5. Conclusions

This paper analyzed the factors affecting the displacements of the connectors and wall panels and modified the corresponding displacement model. The following conclusions can be drawn.

(1) The reduction of the keel spacing could improve the out-of-plane stiffness of the wall panels but has little effect on the stiffness of the connectors.
(2) The increase in the number of screws connecting the L-shaped steel angles to the steel beams can result in significant increases in the out-of-plane stiffnesses of the connectors and wall panels. When the number of screws reaches four or more, the stiffness enhancement effect of the connectors and wall panels will be weakened. In addition, increasing the thickness of the L-shaped steel angles can also improve the

out-of-plane stiffnesses of the connectors and the wall panel, but the improvement effect is gradually insignificant when the thickness reaches a certain threshold.

(3) The increase in the number of special-shaped steel angle connectors can result in significant increases in the out-of-plane stiffnesses of the connectors and wall panels. When the number of connectors reaches three or more, the stiffness enhancement effect of the connectors and wall panels will be weakened.

(4) For the L-shaped steel angle connectors, the pre-proposed displacement model would overestimate the contribution of the number of screws to the rotational stiffness, making the calculation results smaller. The accuracy of the displacement model could be improved by modifying the rotation constraint coefficients of the L-shaped steel angle connectors.

(5) For the wall panel, the ideal articulation constraints assumed by the pre-proposed displacement model would bias the calculations, and thus the introduction of the discount factor could improve the accuracy of the wallboard displacement model.

Overall, in future construction designs, suitable connectors should be selected as required. Increasing the number of connectors and self-tapping screws can quickly improve the out-of-plane stiffnesses of special-shaped and L-shaped connectors and wall panels. The more accurate displacement calculation model provided in this paper can provide an important reference for future construction design.

Author Contributions: Conceptualization, R.G. and A.W.; methodology, R.G.; software, R.G.; validation, R.G., A.W. and H.L.; formal analysis, A.W.; investigation, J.L.; resources, K.L.; data curation, A.W.; writing—original draft preparation, R.G.; writing—review and editing, A.W.; visualization, R.G.; supervision, A.W.; project administration, A.W.; funding acquisition, A.W. All authors have read and agreed to the published version of the manuscript.

Funding: This research was supported by the Key Scientific and Technological Projects of Henan Higher Education (Grant No. 23B560015) and Key Scientific and Technological Projects of Henan Province 2022 (Grant No. 222102320267).

Institutional Review Board Statement: Not applicable.

Informed Consent Statement: Not applicable.

Data Availability Statement: The data presented in this study are available on request from the corresponding author.

Acknowledgments: All authors thank the editors and reviewers for their work on this manuscript.

Conflicts of Interest: Hao Li was employed by the company Xi'an Noble Metal Material Co., Ltd. The remaining authors declare that the research was conducted in the absence of any commercial or financial relationships that could be construed as a potential conflict of interest.

Notation

B_S	Combined stiffness of the wall panel
b	Wall plate section width
c	Distance from the center of the steel beam connecting screws to the line of shear effect
D_0	Lateral displacement stiffness
E	Modulus of elasticity of the connectors
E_S	Modulus of elasticity of the light steel keel
I	Moment of inertia of the connectors
I_S	Sum of the moments of inertia of the keel
I'_1	Moment of the inertia of the phenolic panels
K_b	Overall rotation constraint coefficient of the special-shaped steel angle connectors
k_a	Rotation constraint coefficient of the L-shaped steel angle connector
k_b	Rotation constraint coefficient of a single special-shaped steel angle connector
l_0	Calculated span of the wall panel
m	Mask combination effect coefficient

N	Number of special-shaped steel angle connectors
n_t	Number of screws connecting L-shaped steel angle connectors to steel beams
n_1	Number of extraction-resistant screws
n_2	Number of shear-resistant screws
t_a	Thickness of the L-shaped steel angle connector
t_b	Thickness of the special-shaped steel angle connectors
w_k	Load
γ	Discount factor
Δ	Displacement of the wall panel
Δa	Displacement of L-shaped steel angle connector
Δb	Displacement of special-shaped steel angle connectors

References

1. Yu, Y.Q.; Ma, X.F.; Zhang, A.L.; Wang, Z. Research summary on seismic performance of prefabricated steel plate shear wall structure. *J. Build. Struct.* **2021**, *51*, 16–24. [CrossRef]
2. Xia, Z.; Zhu, L.M.; Han, L.Y.; Du, W.X. Classification and research status of exterior wall of prefabricated steel structure building. *J. Henan Univ.* **2021**, *51*, 728–738.
3. Liang, X.J.; Wang, Y. State-of-the-art on semi-rigid connections for fabricated steel structures. *Prog. Steel Build. Struct.* **2022**, *24*, 1–14.
4. Liu, H.B.; He, X.H.; Gao, L.; Li, F. Numerical simulation of the wind field of assembled steel truss bridge. *Appl. Mech. Mater.* **2013**, *340*, 841–847. [CrossRef]
5. Roy, K.; Ananthi, G.B.G. *Sustainable Composite Construction Materials*; MDPI: Bern, Switzerland, 2023. [CrossRef]
6. Kanagaraj, B.; Nammalvar, A.; Andrushia, A.D.; Gurupatham, B.G.A.; Roy, K. Influence of nano composites on the impact resistance of concrete at elevated temperatures. *Fire* **2023**, *6*, 135. [CrossRef]
7. Ye, J.H. An introduction of mid-rise thin-walled steel structures: Research progress on cold-formed steel framed composite shear wall systems. *J. Harbin Inst. Technol.* **2016**, *48*, 1–9. [CrossRef]
8. Paul Thanaraj, D.; Kiran, T.; Kanagaraj, B.; Nammalvar, A.; Andrushia, A.D.; Gurupatham, B.G.A.; Roy, K. Influence of heating-cooling regime on the engineering properties of structural concrete subjected to elevated temperature. *Buildings* **2023**, *13*, 295. [CrossRef]
9. Zhang, A.L.; Hu, T.T.; Liu, X.C. The classification and comparative analysis of the matching external wall for the prefabricated steel structure residence. *Ind. Constr.* **2014**, *44*, 7–9. [CrossRef]
10. Zhao, B. Crack causes analysis of filler wall of some steel structure masonry. *Constr. Technol.* **2009**, *S1*, 397–398.
11. Mehrabi, A.B.; Shing, P.B.; Schuller, M.P.; Noland, J.L. Experimental evaluation of masonry-infilled RC frames. *J. Struct. Eng.* **1996**, *122*, 228–237. [CrossRef]
12. Naserpour, A.; Ghanbari, M.A.; Haseli, B. Seismic performance of precast concrete walls with replaceable steel slit connections for high-rise buildings. *Innov. Infrastruct. Solut.* **2024**, *9*, 47. [CrossRef]
13. Zhao, Y.; Li, Z.; Liu, P.; Ma, H. The seismic behaviors of steel-concrete-steel composite walls with dumbbell-shaped connectors. *J. Constr. Steel. Res.* **2023**, *211*, 108182. [CrossRef]
14. Lu, Y.L.; Jiang, L.Y.; Lin, F. Seismic performance of precast concrete shear wall using grouted sleeve connections for section steels reinforced at wall ends. *Structures* **2023**, *57*, 105068. [CrossRef]
15. Geng, Y.; Wang, Y.Y.; Ding, J.Z. Mechanical behavior of connections between out-hung light-gauge steel stud walls and steel frames. *J. Build. Struct.* **2016**, *37*, 141–150. [CrossRef]
16. Tang, Z.; Zha, X.; Wang, B. Finite element study on shear performances of in-filled bolt joint of assembled GRC wall with light steel skeleton frame. *IOP Conf. Ser. Earth. Env. Sci.* **2019**, *267*, 042094. [CrossRef]
17. Heimbs, S.; Pein, M. Failure behaviour of honeycomb sandwich corner joints and inserts. *Compos. Struct.* **2009**, *89*, 575–588. [CrossRef]
18. Tian, Y.; Guan, H.; Shao, S.; Yang, Q. Provisions and comparison of Chinese wind load standard for roof components and cladding. *Structures* **2021**, *33*, 2587–2598. [CrossRef]
19. Bui, T.L.; Bui, T.T.; Bui, Q.B.; Limam, A. Out-of-plane behavior of rammed earth walls under seismic loading: Finite element simulation. *Structures* **2020**, *24*, 191–208. [CrossRef]
20. Zhang, Y.; Liu, P.; Zhao, X.F. Structural displacement monitoring based on mask regions with convolutional neural network. *Constr Build Mater.* **2021**, *267*, 120923. [CrossRef]
21. Chai, H.Y.; Ba, P.F.; Qiao, W.T.; Wang, Q. Analysis and experimental study of vertical ultimate load bearing capacity of light steel dense-ribbed walls. *New Build. Mater.* **2024**, *51*, 14–20.
22. Xu, Q.; Lu, W.H.; Wang, M.; Meng, Z.B. Experimental study on effect of initial deformation on shear capacity of W-shaped light steel floor. *Build. Sci.* **2023**, *39*, 127–135.
23. Bian, J.L.; Cao, W.L.; Wu, Z.Y. Experimental study on the seismic performance of composite wall of light steel and tailings microcrystal foamed plate. *World. Earthq. Eng.* **2023**, *39*, 75–87. [CrossRef]

24. Zhao, S.X.; Fan, Q.C.; Zhang, Z.Q.; Peng, M.; Li, Y. Study on bond-slip behavior in lightweight steel and lightweight concrete composite column. *Build. Sci.* **2022**, *38*, 151–157+182.
25. Wu, F.W.; Li, Y.Q. Numerical simulation on shear performance and conversion method considering height to width ratio effect of cold-formed steel framing walls using OpenSees. *J. Build. Struct.* **2023**, *44*, 225–235. [CrossRef]
26. Nassiraei, H.; Rezadoost, P. Initial stiffness, ultimate capacity and failure mechanisms of tubular X-joints with external ring or plates at fire conditions. *Ships. Offshore Struc.* **2024**, *236*, 2317656. [CrossRef]
27. Telue, Y.; Mahendran, M. Behavior of cold-formed steel wall frames lined with plasterboard. *J. Constr. Steel. Res.* **2001**, *54*, 435–452. [CrossRef]
28. Tian, Y.S.; Wang, J.; Lu, T.J. Racking strength and Stiffness of Cold-formed Steel Wall Frames. *J. Constr. Steel. Res.* **2004**, *60*, 1069–1093. [CrossRef]
29. Chou, S.M.; Chai, G.B.; Ling, L. Finite element technique for design of stub columns. *Thin Wall Struct.* **2000**, *37*, 97–112. [CrossRef]
30. Wang, J.C.; Qiu, Z.M.; Liang, J.H. Experimental investigations on the lateral performance of foam concrete light steel keel composite wall. *J. Build. Eng.* **2023**, *72*, 106551. [CrossRef]
31. Peng, H.J.; Luo, D.; Deng, X. Study on integral assembled light steel keel external wall panel. *Guangdong Archit. Civ. Eng.* **2019**, *26*, 92–95.
32. Zou, X.Y.; Li, K. Research on lateral performance of the connection between light steel keel fireproof exterior wall and steel frame. *J. Build. Struct.* **2023**, *53*, 146–152. [CrossRef]
33. Li, K.; Wang, L.; Tang, W.L.; Wang, X.L. Analysis on out-of-plane mechanical behaviors of lightweight steel keel fireproof exterior wall and its connection with steel frame. *J. Build. Struct.* **2023**, *53*, 127–135. [CrossRef]
34. Zhang, H.X.; Li, G.C.; Yang, P. FEM analysis on out-of-plane mechanical performance of light steel interior wall with new type connection. *Steel. Constr.* **2016**, *31*, 53–58. [CrossRef]
35. Bao, W.; Guo, R.; Yuan, S. Lateral force resistance behavior of semi-rigid steel frame with light steel keel wall. *J. Build. Struct.* **2013**, *34*, 154–160.
36. Balik, F.S.; Bahadir, F.; Kamanli, M. Seismic Behavior of lap splice reinforced concrete frames with light-steel-framed walls and different anchorage details. *Struct. Eng. Int.* **2023**, *33*, 488–497. [CrossRef]

Disclaimer/Publisher's Note: The statements, opinions and data contained in all publications are solely those of the individual author(s) and contributor(s) and not of MDPI and/or the editor(s). MDPI and/or the editor(s) disclaim responsibility for any injury to people or property resulting from any ideas, methods, instructions or products referred to in the content.